Eur. Phys. J. D **40**, 27–35 (2006)
DOI: 10.1140/epjd/e2006-00189-8

THE EUROPEAN PHYSICAL JOURNAL D

Ionization and plasma formation in high n cold Rydberg samples

W. Li[a], P.J. Tanner[b], Y. Jamil[c], and T.F. Gallagher

Department of Physics, University of Virginia, McCormick Road, Charlottesville, VA 22904, USA

Received 1st December 2005 / Received in final form 12 June 2006
Published online 18 August 2006 –

Abstract. The experiments reported here show that the dipole-dipole interaction, the fundamental interaction between the cold Rydberg atoms, is the dominant initial ionization mechanism for evolution from a frozen Rydberg gas into a plasma. The study also indicates that plasma formation follows a path of initial ionization, redistribution of Rydberg population to higher angular momentum states, and rapid avalanche ionization due to electron-Rydberg collisions.

PACS. 32.80.Pj Optical cooling of atoms; trapping – 34.60.+z Scattering in highly excited states

1 Introduction

Cold dense samples of Rydberg atoms exhibit many fascinating collective phenomena normally associated with solids and other dense physical systems. On the 1 μs time scale of experimental interest, the 300 μK atoms move only 0.3 μm, roughly 3% of the average interatomic spacing at a density of 10^9 cm^{-3}. Due to their large dipole moments, scaling as n^2, where n is the principal quantum number, these cold Rydberg atoms interact as in a disordered solid [1–6]. These strong but controllable interactions between cold Rydberg atoms have been suggested as the basis for gates for quantum computing [7,8]. Cold Rydberg atom samples have also been observed to spontaneously evolve into ultracold plasmas, and ultracold plasmas recombine to form Rydberg atoms [9–12].

A plasma forms spontaneously from cold Rydberg atom samples as follows [9]. The cold Rydberg atoms are first ionized through one or more initial ionization mechanisms; the liberated electrons leave the trap volume instantly, but the cold ions are left behind. Once enough, typically ∼1000, ions accumulate, the potential well from their macroscopic positive charge traps subsequently produced electrons. The collisions between the trapped electrons and the cold Rydberg atoms lead to avalanche ionization, which quickly redistributes the Rydberg population from the initial Rydberg state. Roughly 2/3 of the initial Rydberg atoms are ionized to form the ultracold plasma; the remaining 1/3 are transferred to lower lying states, providing energy balance [13]. For low n, $n < 40$, states, the initial ionization comes predominantly from photoionization by 300 K blackbody radiation or collisions with residual 300 K Rydberg atoms. At high n, $n > 40$, even when there are no hot atoms the evolution to a plasma occurs more rapidly than at low n, and the rate for the initial ionization process scales as n^4 [13], which is inconsistent with a 300 K blackbody photoionization rate. It is the scaling typical of Rydberg-Rydberg collisions, but there are initially no moving atoms. It has recently been shown that the attractive dipole-dipole interaction between cold Rydberg atoms leads to their moving toward each other and colliding to produce the initial ions necessary for forming a plasma [14]. Here we present the results of more detailed and extensive experiments on the dipole-dipole interaction as the initial ionization mechanism for plasma formation. We briefly summarize how dipole-dipole interaction initiates plasma formation, describe the experimental results leading to this picture, and conclude with the implications.

2 Dipole-dipole ionization and plasma formation

The fundamental interactions between two neutral atoms are their electric multipole interactions, and the longest range of these is the dipole-dipole interaction [15]. We consider molecular states composed of two atoms, and we write the molecular state wave function as direct product of two atomic wave functions i.e. $|12\rangle = |1\rangle\,|2\rangle$. For example, we write the state $|44d44d\rangle$ as $|44d\rangle\,|44d\rangle$, and it has the energy $W_{44d44d} = W_{44d} + W_{44d}$. We are interested in the electric dipole couplings of this state to other states,

[a] *Present address:* Physics and Astronomy Department, Rice University, Houston, TX 77005, USA.
[b] e-mail: pjt3d@virginia.edu
[c] *On leave from* Department of Physics, University of Agriculture, Faisalabad, Pakistan.

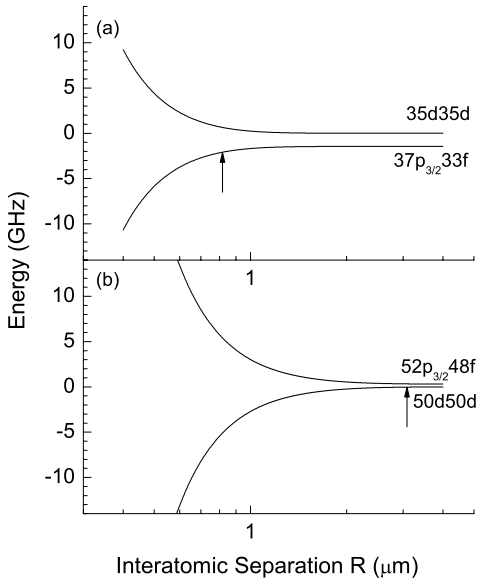

Fig. 1. Interaction between pairs of (a) $35d$ and (b) $50d$ atoms and their near resonant pf pairs. $R_{\rm vdW}$ occurs where $V = \mu_1\mu_2/R^3 = \Delta$, which is (a) 0.8 μm for $35d$ and (b) 2.1 μm for $50d$ pairs as indicated by the arrows.

which must be $|nln'l'\rangle$ states where l and l' are p or f states. The most important couplings are those to $|nln'l'\rangle$ states which satisfy two criteria. First, they have energies $W_{nln'l'}$ close to W_{44d44d}, so that they are nearly degenerate, and second, n and n' must be near 44 so the dipole matrix elements coupling the nl and $n'l'$ state to the $44d$ state, μ_1 and μ_2, for the two atoms are large.

As an example we consider the initial state to be $|dd\rangle$, with energy $W_{dd} = 0$. The nearest dipole coupled state is pf which has energy $W_{pf} = \Delta$. We take the coupling to be

$$V(R) = \frac{\mu_1\mu_2}{R^3}, \tag{1}$$

where $\mu_1 = \langle d\,|\mu|\,p\rangle$ and $\mu_2 = \langle d\,|\mu|\,f\rangle$. For simplicity we ignore all orientational effects and symmetrization of the wavefunction. In this approximation the Hamiltonian of the system can be written as

$$H = \begin{pmatrix} 0 & V(R) \\ V(R) & \Delta \end{pmatrix}. \tag{2}$$

It is useful to note that both μ_1 and μ_2 scale as n^2, and $\Delta \approx \delta/n^3$, where δ depends on the atomic quantum defects. To a first approximation $\delta = 2\delta_d - \delta_p - \delta_f$ (mod 1), and we choose the value of δ for which $|\delta|$ is minimized. Here δ_d, δ_p, and δ_f are the quantum defects of the atomic d, p, and f states. The eigenvalues of the Hamiltonian are

$$\lambda_{1,2} = \frac{\Delta \pm \sqrt{\Delta^2 + 4V^2}}{2}, \tag{3}$$

and examples are plotted in Figure 1 as a function of interatomic separation, R.

At large R, where the dipole coupling term is much smaller than the detuning, $V \ll \Delta$, the eigenvalues can be approximated as

$$\lambda_1 \approx \Delta + \frac{V^2}{\Delta}, \quad \lambda_2 \approx -\frac{V^2}{\Delta}. \tag{4}$$

The energy shifts due to the interaction are $\pm V^2/\Delta \sim n^{11}/R^6$. Summing over all such terms gives the van der Waals interaction, which has a $1/R^6$ dependence. It is dominated by the near resonant term we are considering, and thus exhibits an n^{11} scaling. It can be seen that the van der Waals interaction is essentially the off-resonance dipole coupling calculated by second order perturbation theory. However, at small R, where the dipole coupling term is much larger than the detuning, $V \gg \Delta$, the eigenvalues can be approximated as

$$\lambda_{1,2} \approx \pm V. \tag{5}$$

The energy shifts due to the interaction are $\pm V \sim n^4/R^3$, which is essentially a resonant dipole-dipole interaction. The transition from van der Waals interaction to dipole-dipole interaction occurs in the region where the dipole coupling term is equal to the detuning term, $V = \Delta$. The arrows in Figure 1 indicate the transition separation, which we label $R_{\rm vdW}$, defined by $\Delta = \mu_1\mu_2/R_{\rm vdW}^3$. For $\mu_1\mu_2 = n^4$ and $\Delta = \delta/n^3$,

$$R_{\rm vdW} \approx \left(\frac{n^7}{\delta}\right)^{1/3}. \tag{6}$$

Apparently, states with different detunings have different transition distances. However, as long as the atoms are closer than the transition distance, the dipole-dipole interaction will always dominate. In the special case where the two molecular states are degenerate at infinite separation, that is $\Delta = 0$, the interaction will be dipole-dipole in nature for all R. As shown in Figure 1a, the van der Waals part of the potential curve is flat, compared to the dipole-dipole region. Therefore the atoms in the dipole-dipole interaction regime feel a strong force and are quickly drawn to each other and collide [14]. As demonstrated by the experiments described in Section 4, the closely spaced atoms with attractive dipole-dipole interactions are critical for spontaneous plasma formation from cold Rydberg atoms.

The experiments have shown that (1) from a sample of cold nd state atoms of ^{85}Rb, a plasma forms much more quickly with higher n ($n \sim 40$–50) than with lower n ($n \sim 30$–40) even when there are only cold atoms and (2) a plasma forms much more quickly from nd atoms than from energetically nearby $n's$ atoms of comparable density [14]. Both observations can be explained by their dipole-dipole interactions.

Let us consider the case of high vs. low nd atoms. A pair of $ndnd$ atoms is dipole coupled to all molecular states

in which the same atoms are in f or p states. The dominant coupling is to the energetically nearby state with smallest detuning Δ, which, in this case, is the $(n+2)p_{3/2}(n-2)f$ state. Figure 1 shows the potential curves of (a) dipole coupled $35d35d$ and $37p_{3/2}33f$ pairs and (b) dipole coupled $50d50d$ and $52p_{3/2}48f$ pairs. The detuning Δ of the $52p_{3/2}48f$ state from the $50d50d$ state at $R = \infty$ is 300 MHz [16], and the dipole moments are $\mu_{dp} = 1840$ and $\mu_{df} = 1893$, which we calculate by the Numerov method [17]. Unless units are given explicitly, all quantities will be expressed in atomic units. This results in $R_{\rm vdW} = 2.1$ μm for $50d$ atoms as indicated by the arrow in Figure 1b. The detuning Δ of the $37p_{3/2}33f$ state from the $35d35d$ state at $R = \infty$ is –1.443 GHz [16], and the dipole moments are $\mu_{dp} = 875$ and $\mu_{df} = 882$, respectively. Consequently, $R_{\rm vdW} = 0.8$ μm for $35d$ atoms as indicated by the arrow in Figure 1a. A pair of atoms initially on the attractive curve are drawn to each other, collide, and ionize, providing the initial ionization required for the evolution to plasma. If there are 10^5 atoms in a sphere of 0.1 mm radius, roughly 1500 atoms must be ionized to provide the macroscopic space charge needed for avalanche ionization. For $50d$ atoms, the most closely spaced 1500 atoms, separated by $R \leq 1.7$ μm, are all in the resonant dipole-dipole interaction regime. A simple kinematic calculation determines atoms initially separated by $R \leq 1.7$ μm will collide with each other within 300 ns when they move on the attractive potential curve; generating an ion, an electron, and a more tightly bound atom. For simplicity of calculation, a collision is assumed to occur when the interatomic separation equals the Rydberg diameter. The ion and the atom generated this way are not necessarily cold and may have temperatures of tens of Kelvin.

A similar argument holds for the observation that a plasma forms much more quickly from nd states than from energetically nearby $n's$ states [14]. It is useful to note that the potential curves for the Rb $np_{3/2}$ states, which also easily form a plasma, resemble the high-lying ($n > 40$) Rb nd curves.

After initial ionization, the free ions accumulated in the trap redistribute the initially excited Rydberg population. The local and macroscopic electric fields from the ions quickly produce high ℓ states via Stark mixing. Meanwhile the macroscopic electric field captures consequently liberated electrons, and the sample evolves to a plasma through collisions between these electrons and cold Rydberg atoms.

3 Experimental approach

The experimental set-up is the same as in reference [14]. We start with ^{85}Rb atoms in a vapor loaded MOT, in which the atoms are at 300 μK and a $5p_{3/2}$ density of 5×10^{10} cm^{-3} [18]. The atoms are excited from the $5p_{3/2}$ state to ns or nd Rydberg states at a 20 Hz repetition rate using a pulse amplified, frequency doubled 960 nm continuous wave Ti:sapphire laser. The laser pulses have 10 ns duration, 20 μJ energy, and 200 MHz bandwidth, and the beam is focused to a 0.2 mm diameter waist in the trap volume. About 10% of the cold atoms are excited to Rydberg states, leading to a maximum density of Rydberg atoms of 5×10^9 cm^{-3}. The atoms may or may not be exposed to a short microwave pulse. The sample then evolves spontaneously for a certain amount of time which we term the delay time. The final states of the system are analyzed by SFI (selective field ionization) by means of a field ramp and time resolved detection. Depending on the configuration, either ions or the electrons can be detected. Electrons freed due to initial dipole-dipole induced collisions quickly leave the trapping region and cannot be detected. By detecting ions, the free ions produced before plasma formation can be measured; by detecting electrons, we can determine if a plasma is formed and also measure the high ℓ states and the low lying states by SFI.

4 Observations

4.1 Dipole-dipole transitions from nd states

As discussed in Section 2, the attractive dipole-dipole interaction is responsible for initially generating ions. A pair of $ndnd$ atoms is dominantly dipole-dipole coupled to the $(n+2)p_{3/2}(n-2)f$ state, the energetically nearest state. Close pairs of nominally dd atoms will either repel each other if they are on the repulsive dipole-dipole curve, or move toward each other, collide, and ionize, if they are on the attractive dipole-dipole potential. Since this is a binary process through the dipole-dipole interaction, we expect the total population transferred to either the p state or free ions to be proportional to the square of the total initial Rydberg population density, N^2, and have an n^4 dependence on the principal quantum number n. To verify these predictions, we take the time resolved SFI spectra of ions for a series of densities for a few different nd states, at 250 ns delay after laser excitation, when free ions are produced by the dipole-dipole interaction, but a plasma has not yet formed from avalanche ionization. Shown in Figure 2 are the time resolved ion signals from the $46d$ state at 250 ns delay for two different densities. At the higher density of Figure 2a, both the signals from the free ions due to dipole-dipole induced ionization and from the $48p$ state by the resonant dipole-dipole interaction from the $46d$ state are substantial. At the lower density of Figure 2b, however, there is only a small $48p$ state signal, and no free ion signal. This agrees with the expectation based on the previous discussion. To show the density dependence of the transfer and/or ionization rate, we plot the ratio of the combined $48p$ and free ion signals, which is the area under the dashed line in Figure 2, to the total signal vs. density for several different densities, as shown in Figure 3. The ratios exhibit the linear dependence on the total number of atoms excited, as expected for a binary process; the slope of the plot is proportional to the nonlinear transfer rate. Also shown in Figure 3 are the results of the analogous measurements for several different d states, $33d$, $38d$, and $42d$. The transfer rates for different states vary, as reflected by their different slopes.

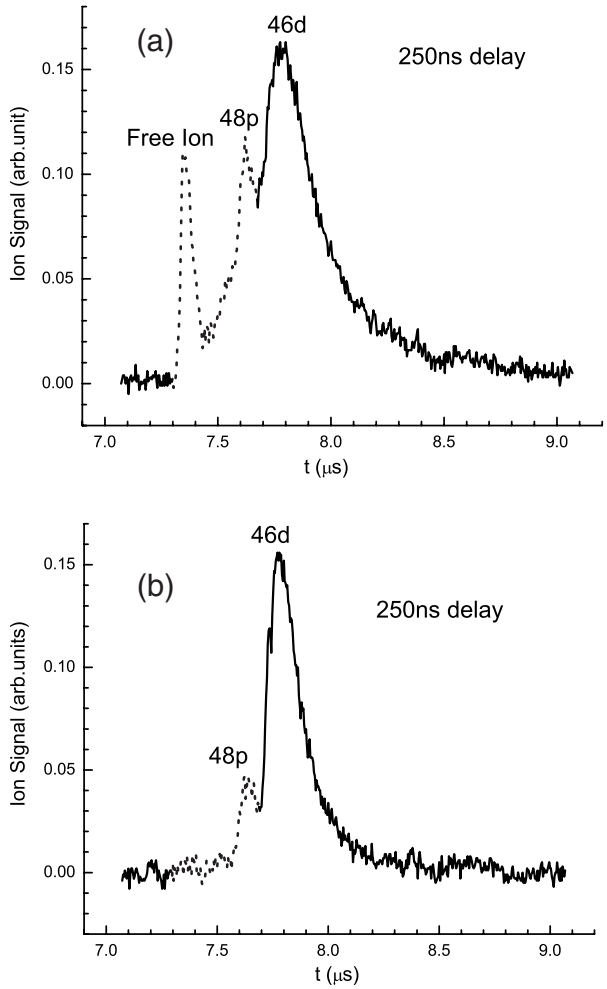

Fig. 2. Time resolved ion signals from 46d excitation with 250 ns field ionization delay for two different densities: (a) 4×10^9 atoms/cm^3; and (b) 2×10^9 atoms/cm^3. The free ion, the 48p state, and the originally excited 46d state are labeled in the figures. The dashed lines are used to indicate the parts of the signals ionized or transferred from the original 46d state.

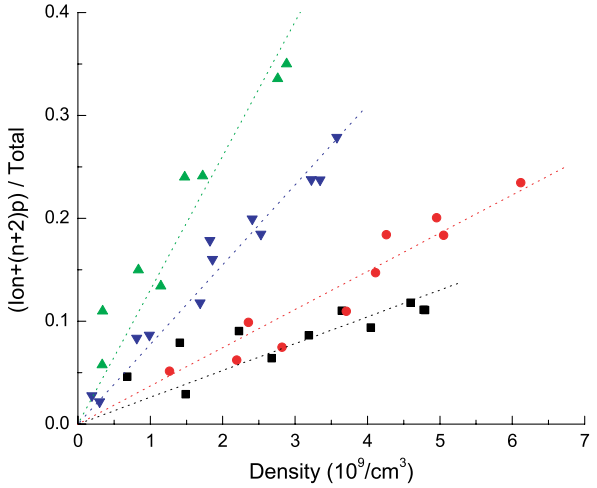

Fig. 3. Ratio of the free ion + $(n{+}2)p$ signals produced by the resonant dipole-dipole interaction to the total signal detected 250 ns after laser excitation of the 33d (■), 38d (●), 42d (▲), and 46d (▼) states. The slopes of the ratios are linear in the number of atoms, as expected for a binary process.

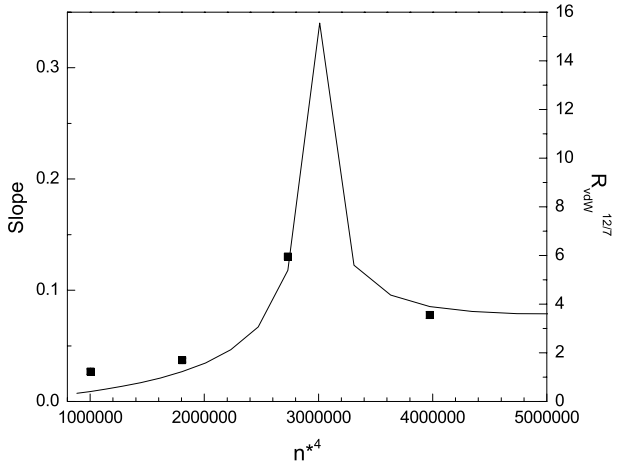

Fig. 4. Slope extracted from Figure 3 vs. $n*^4$, where $n* = n - \delta_d(n)$. The slope (left panel) is proportional to the nonlinear transfer rate. The fitting curve is $R_{\rm vdW}^{12/7}$ plotted against $n*^4$ (right panel), where $R_{\rm vdW}^{12/7} \propto n*^4$ as discussed in the text.

It was initially surprising to us to see that the ionization rate for the 42d state was higher than that of 46d state, as shown in Figure 4. We expected a monotonic dependence on n. However the parameter Δ (the detuning between $(n+2)p$ $(n-2)f$ and $ndnd$) changes sign at $n = 43$, so $R_{\rm vdW}$ does not exhibit the simple $n^{7/3}$ scaling of equation (6) but has a resonance at $n = 43$. To be more precise, we should use $n* = n - \delta_d(n)$, the effective principal quantum number, and transfer rates are plotted against $n*^4$ in Figure 3. The solid fitting curve is the scaled van der Waals distance $R_{\rm vdW}$, as defined earlier, vs. $n*^4$. It is not completely clear that the calculated curve should match the experimental points, but it does. It will be most interesting to see if the 43d ionization rate matches the peak of the calculated curve.

4.2 Laser spectroscopy of dipole-dipole interactions

We interpret the plasma formation from initially excited nd atoms to the motion along the *attractive* dipole-dipole potential as illustrated in Figure 1. Therefore, we should observe more ionization on the red side of the optical excitation of the nd state than on the blue side of it and is shown qualitatively by the time resolved ion signals in Figure 5. In this figure, the blue pulsed laser exciting the 46d state is manually set to two different frequencies separated by about 50 MHz, but the absolute values of the frequencies are unknown. The signals of the low laser frequency are on the left column, and the signals of the high laser frequency are on the right column. At a delay of 250 ns, as shown by the two signals in upper row, the overall

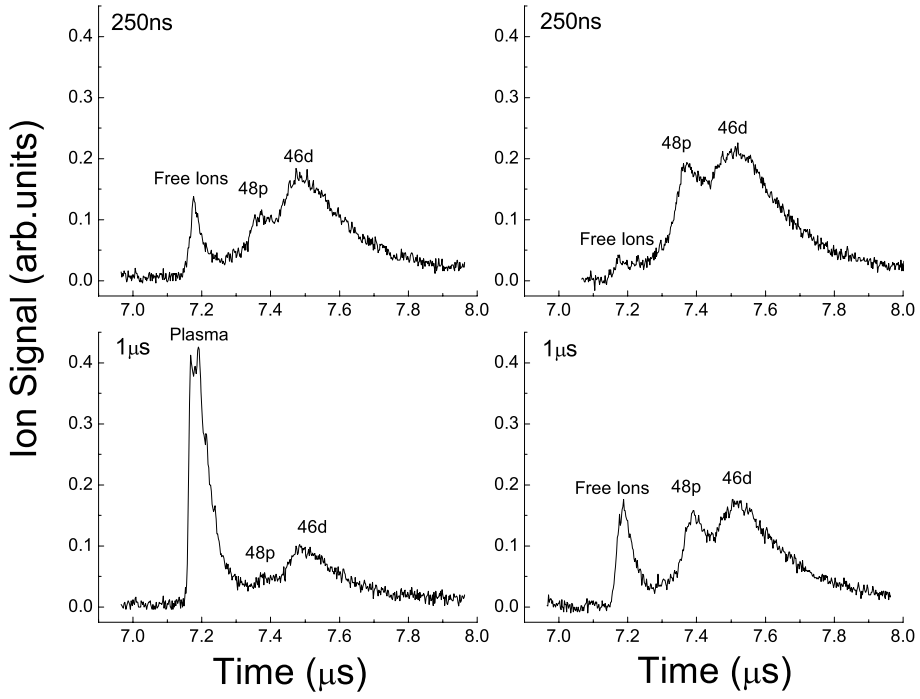

Fig. 5. Ion and plasma formation with high and low frequencies of the pulsed blue laser relative to the $5p_{3/2} \rightarrow 48d_{5/2}$ transition at two different delay times: 250 ns and 1 μs. The spectra in the left column are taken with low laser frequency, and the spectra in the right column are taken with high laser frequency. The separation between the high and low frequencies is about 50 MHz, however, the absolute frequencies are unknown. The initial density of $46d$ atoms is always 4×10^9 atoms/cm^3. The free ion and plasma signals are differentiated by also looking at electron spectra (not shown).

population transfer from the initial $46d$ state to the $48p$ state and the free ions together is about the same in both cases. However, there are many more free ions formed from the low laser frequency excitation than from the high laser frequency excitation. Consequently, the population transfer to the $48p$ state is higher in the high laser frequency case. This does agree with the picture that the ionization is from the attractive dipole-dipole interaction between the atoms: when the atoms are excited by the low laser frequency to the attractive side of the potential curve, the atoms are pulled together and collide to form ions; when the atoms are excited by the high laser frequency to the repulsive side of the potential curve, the atoms are only slightly pushed away from each other, and they most likely do not make a resonant energy transfer to the $48p$ state. At 1 μs, as shown by the two spectra in the lower row, for the sample excited by the low laser frequency, a plasma has already formed, but for the sample excited by the high laser frequency, the accumulated free ions are still slightly under the threshold of plasma formation.

4.3 Microwave spectroscopy of dipole-dipole interactions

Ionization on the attractive dipole-dipole potential can be shown with unprecedented clarity using microwaves. To show the ionization on the attractive dipole-dipole potential using microwaves, we start with atoms laser excited to the $39s$ state. Samples in this state do not spontaneously evolve into a plasma until more than 10 μs have elapsed. For the experimental procedure, the only extra step from the previous plasma experiments is to add a microwave pulse between the laser excitation and the field ionization pulse. Both the duration of the microwave pulse and the delay time before the field ionization pulse can be easily adjusted.

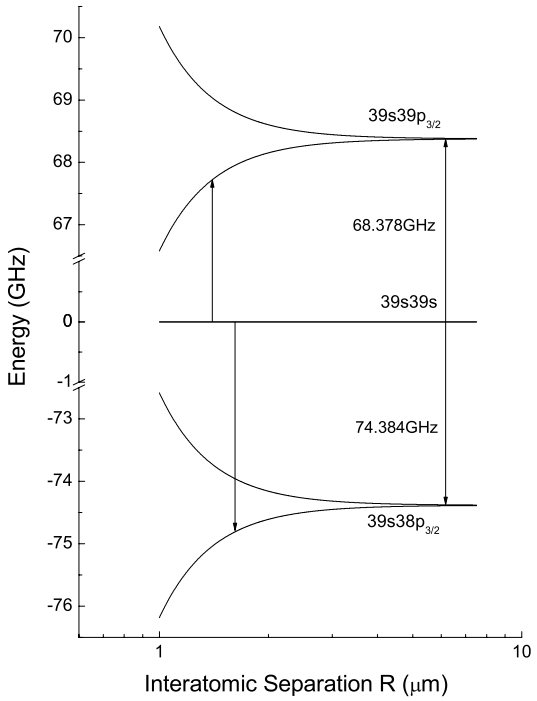

Fig. 6. Energy levels of the $39s39s \rightarrow 39s39p_{3/2}$ and $39s38p_{3/2}$ states vs. interatomic spacing R. The atomic transition frequencies between $39s$ and $38p_{3/2}$, $39p_{3/2}$ are 74.384 and 68.378 GHz as indicated.

Shown in Figure 6 are the energy levels for the $39s39s$–$39s39p_{3/2}$ and $39s39s$–$39s38p_{3/2}$ transitions vs. interatomic spacing R. The atomic transition frequencies of

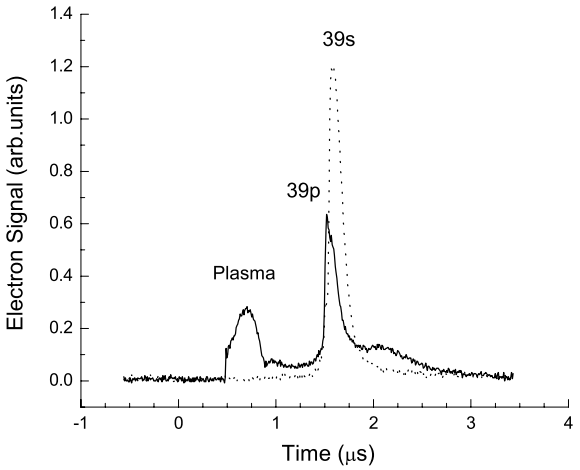

Fig. 7. Time resolved electron signals taken 3.5 μs after exciting the 39s state with (—) and without ($\cdots$) the microwave pulse. In both cases, the initial density of the 39s state is 5×10^9 atoms/cm^3. Without the microwaves only the 39s field ionization signal is observed. With the microwave pulse a plasma signal and redistribution of the remaining Rydberg population are evident.

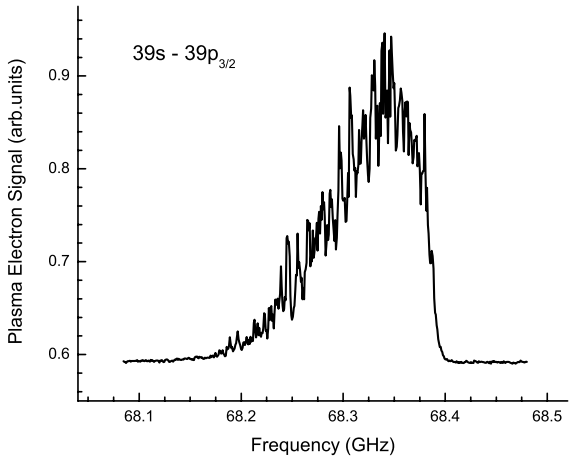

Fig. 8. Plasma electron signal vs. microwave frequency. The microwave pulse duration is 500 ns, and the field ionization delay is 3.5 μs. Plasma signal is only observed on the low frequency side of the 39s $\rightarrow$ 39$p_{3/2}$ transition resonance 63.378 GHz, corresponding to the attractive potential in Figure 7.

the 39s–39$p_{3/2}$ and 39s–38$p_{3/2}$ transitions are 68.378 GHz and 74.384 GHz, as indicated in Figure 6. According to the attractive dipole induced ionization mechanism, the sample should evolve into a plasma only if the microwaves drive transitions to the low energy, attractive molecular state, but not the high energy, repulsive molecular state.

In Figure 7, we show the time resolved electron signals detected 3.5 μs after the 39s state is populated with and without a microwave pulse to drive the 39s–39$p_{3/2}$ transition. The microwave pulse is 500 ns long and produces an on resonance Rabi frequency of 50 MHz. The frequency of the microwave pulse is set to be 68.34 GHz, 40 MHz to the red side of the resonance. In Figure 7, both with and without microwave pulses, the same number of 39s atoms is excited. Without the pulse, the population remains in the 39s state after a 3.5 μs delay, but with it, a plasma does form as shown in the time resolved signal of Figure 7. There is obvious population transfer to other Rydberg states as well. In this case, we are in fact really driving the molecular transition from the 39s39s state to the attractive 39s39$p_{3/2}$ potential curve, as indicated by the arrow in Figure 6. If we monitor the plasma signal in Figure 7 while scanning the microwave frequency, the resulting microwave spectrum is shown in Figure 8. The spectrum has a clear cutoff at the frequency 68.378 GHz, the resonance of the 39s–39$p_{3/2}$ atomic transition. The plasma only forms on the low frequency side of the atomic transition, corresponding to the attractive side of potential curve in Figure 6, but not on the high frequency side, corresponding to the repulsive side of the potential curve. To further verify that the plasma formation on the low frequency side of the atomic transition is indeed due to the attractive dipole-dipole interaction induced ionization, we detect the ion signal at 1 μs after the laser excitation, when a plasma does not yet form, but the free ions generated by

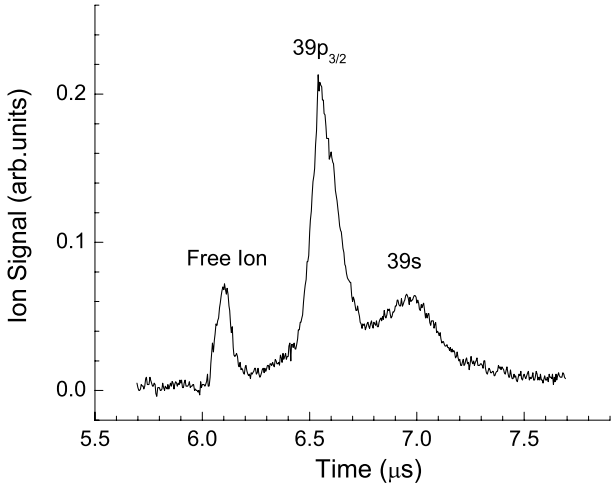

Fig. 9. Time resolved ion signal taken 1 μs after exciting the 39s state. Microwave pulse duration is again 500 ns, the frequency is set to be slightly on the red side of the resonance of 39s $\rightarrow$ 39$p_{3/2}$ transition. The initial density of the 39s state is 5×10^9 atoms/cm^3. At this delay, there is a free ion signal as shown in the figure, but no plasma yet, which is verified by looking at the electron signal.

attractive dipole-dipole interaction are already present, as shown in Figure 9. If we monitor the free ion signal in Figure 9 while scanning the microwave frequency, the resulting spectrum shown in Figure 10 also has the cutoff at the atomic transition frequency. This makes it absolutely clear that the attractive dipole-dipole interaction is the initial ionization mechanism for plasma formation from the cold Rydberg atoms. If we drive the 39s–38$p_{3/2}$ transition using microwaves, and take the spectrum of plasma vs. microwave frequency, not surprisingly, we also see a clear cutoff at the 39s–38$p_{3/2}$ transition frequency of 74.384 GHz, as shown in Figure 11. In this case, the plasma signal is only observed on the high frequency side of the resonance,

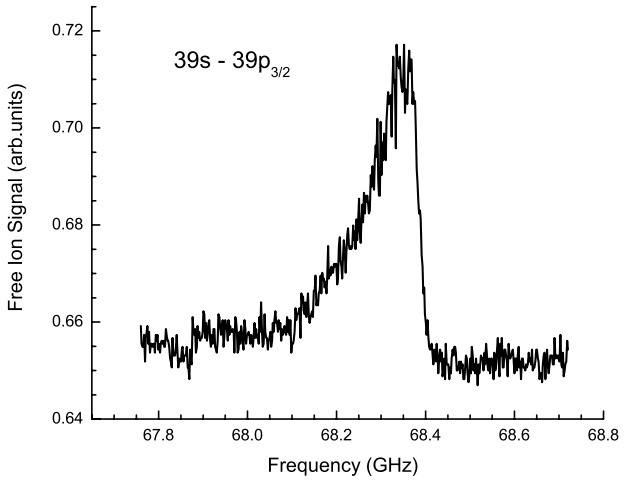

Fig. 10. Free ion signal vs. microwave frequency. The microwave pulse duration is 500 ns, and the field ionization delay is 1 μs. Free ion signal is only observed on the low frequency side of the $39s \rightarrow 39p_{3/2}$ transition resonance at 63.378 GHz.

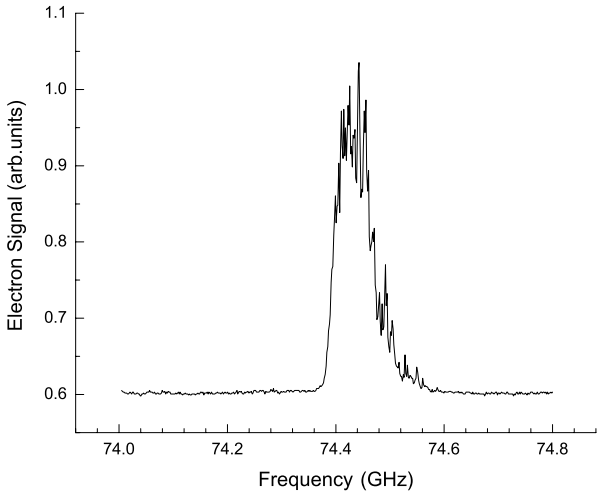

Fig. 11. Plasma electron signal vs. microwave frequency. The microwave pulse duration is 500 ns, and the field ionization delay is 3.5 μs. Plasma signal is only observed on the high frequency side of the $39s \rightarrow 38p_{3/2}$ transition resonance 74.384 GHz, corresponding to the attractive potential in Figure 6.

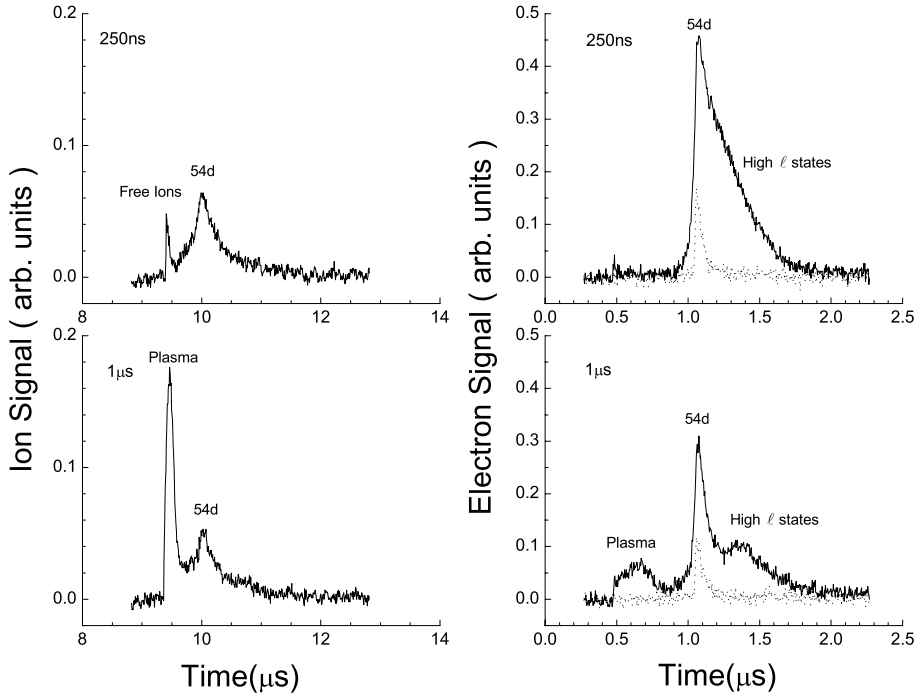

Fig. 12. Dynamics of spontaneous plasma evolution from the 54d state. The initial density of 54d state samples is 2×10^9 atoms/cm^3 for all solid line (—) signals, but 1×10^8 atoms/cm^3 for the dotted line ($\cdots$) signals. Both time resolved ion and electron signals are detected at delay times 250 ns and 1 μs. The two figures in the left column are ion signals, and the two figures in the right column are electron signals.

since for this transition the attractive potential curve has higher frequency than the atomic transition as indicated in Figure 6.

4.4 Plasma evolution from ns and nd states

The dynamics of the spontaneous evolution from nd states to a plasma are shown in Figure 12 by the time resolved signals of both ions and electrons at the same delay time. Free ions are already seen in the ion spectrum 250 ns after laser excitation of the 54d state, but there is barely any plasma in the corresponding electron spectrum. However, there is a high ℓ population present, which can be clearly seen by comparing this spectrum to the very low density signal plotted in the dotted line. Presumably the production of high ℓ states occurs by conversion of nf states into higher ℓ states by the Stark fields due to the ions. Very small fields are required to mix the Rb nf states with the higher ℓ states, $\sim$ 0.17 V/cm at $n = 50$. At 1 μs, the sample evolves into a plasma as shown in both electron and ion spectra.

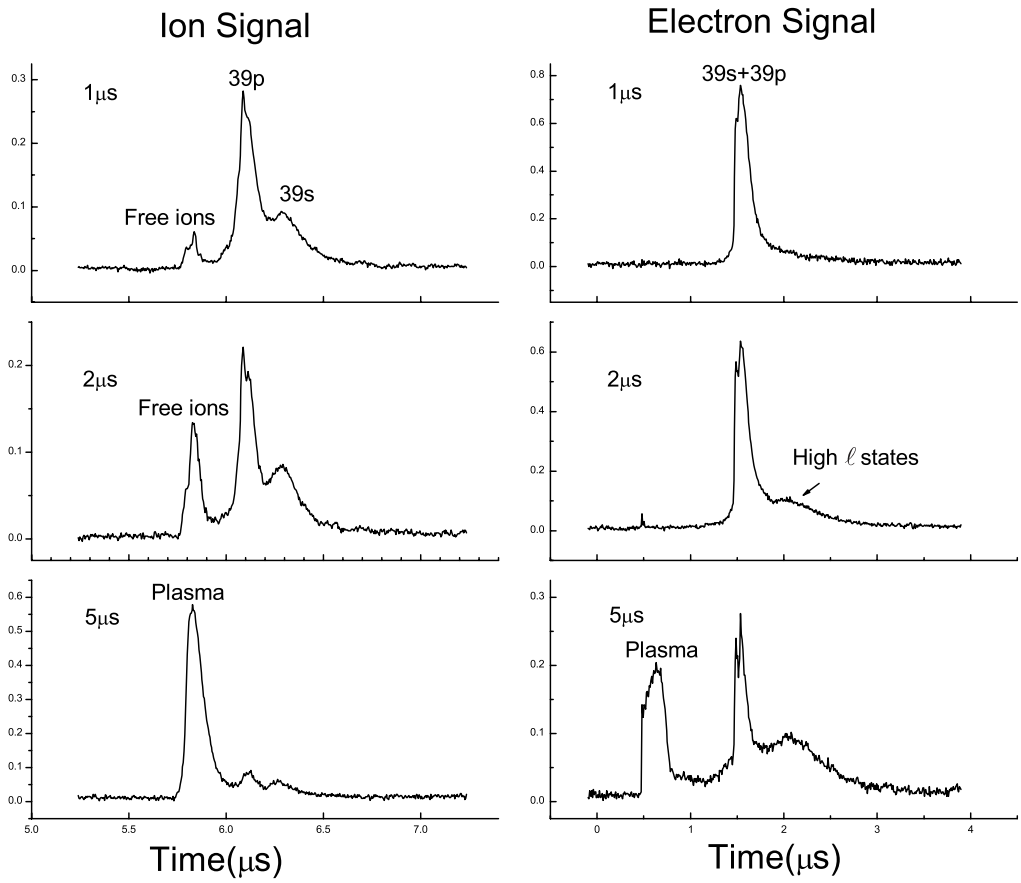

Fig. 13. Dynamics of plasma evolution from the $39s$ state driven by microwave transition. The microwave pulse duration is 400 ns, and the frequency is set to be 68.26 GHz, slightly lower than the atomic resonance of $39s \rightarrow 39p_{3/2}$ transition. The initial density of the $39s$ state is always 5×10^9 atoms/cm^3. Both time resolved ion and electron signals are detected at delay times of 1 μs, 2 μs, and 5 μs. The three figures on the left are ion signals, and the three figures on the right are electron signals.

Plasma evolution dynamics have also been studied by microwave driven dipole-dipole ionization from ns states, as shown in Figure 13. The microwave pulse duration is 400 ns, and the frequency is set to be 68.26 GHz, slightly lower than the frequency of the $39s$–$39p_{3/2}$ atomic transition. Both ion and electron signals are detected as indicated. At 1 μs delay, the free ions due to the attractive dipole-dipole ionization can be seen in the time resolved ion spectrum, but there is no plasma signal in the corresponding electron spectrum; at 2 μs delay, the free ion signal grows much bigger, and a tiny plasma appears, but there is already substantial population transfer to high ℓ states, as shown in the electron spectrum. Again, we presume this to be due to the Stark effect from the electric field from free ions. At 5 μs delay, the sample evolves into a plasma as shown in both electron and ion spectra, and the accompanying population redistribution is clearly seen in the electron spectrum [19,20].

5 Conclusion and implications

In conclusion, these measurements indicate that ionization resulting from the resonant dipole-dipole interaction is the source of the initial ionization leading to the Rydberg-plasma evolution in purely cold atom samples. More generally, the dipole interactions between Rydberg atoms cause them to move, and this motion cannot be neglected in any proposed applications involving cold Rydberg atoms, such as constructing fast quantum logic gates. The motion and subsequent collisions would destroy the necessary sample coherence. This motion may, however, be minimized by using a regular lattice of atoms.

This work has been supported by the Air Force Office of Scientific Research. It is a pleasure to acknowledge stimulating discussions with B.J. Claessens, P. Pillet, and M. Weidemüller.

References

1. W.R. Anderson, J.R. Veale, T.F. Gallagher, Phys. Rev. Lett. **80**, 249 (1998)
2. I. Mourachko, D. Comparat, F. de Tomasi, A. Fioretti, P. Nosbaum, V.M. Akulin, P. Pillet, Phys. Rev. Lett. **80**, 253 (1998)
3. J.S. Frasier, V. Celli, T. Blum, Phys. Rev. A **59**, 4358 (1999)
4. I. Mourachko, W. Li, T.F. Gallagher, Phys. Rev. A **70**, 031401 (2004)
5. T.J. Carroll, K. Claringbould, A. Goodsell, M.J. Lim, M.W. Noel, Phys. Rev. Lett. **93**, 153001 (2004)
6. K. Afrousheh, P. Bohlouli-Zanjani, D. Vagale, A. Mugford, M. Fedorov, J.D.D. Martin, Phys. Rev. Lett. **93**, 233001 (2004)

7. D. Jaksch, J.I. Cirac, P. Zoller, S.L. Rolston, R. Côté, M.D. Lukin, Phys. Rev. Lett. **85**, 2208 (2000)
8. M.D. Lukin, M. Fleischhauer, R. Côté, L.M. Duan, D. Jaksch, J.I. Cirac, P. Zoller, Phys. Rev. Lett. **87**, 037901 (2001)
9. M.P. Robinson, B. Laburthe Tolra, M.W. Noel, T.F. Gallagher, P. Pillet, Phys. Rev. Lett. **85**, 4466 (2000)
10. S.K. Dutta, D. Feldbaum, A. Walz-Flannigan, J.R. Guest, G. Raithel, Phys. Rev. Lett. **86**, 3993 (2001)
11. T.C. Killian, M.J. Lim, S. Kulin, R. Dumke, S.D. Bergeson, S.L. Rolston, Phys. Rev. Lett. **86**, 3759 (2001)
12. E.E. Eyler, P.L. Gould, private communication
13. W. Li, M.W. Noel, M.P. Robinson, P.J. Tanner, T.F. Gallagher, D. Comparat, B. Laburthe-Tolra, N. Vanhaecke, T. Vogt, N. Zahzam, P. Pillet, D.A. Tate, Phys. Rev. A **70**, 042713, (2004)
14. W. Li, P.J. Tanner, T.F. Gallagher, Phys. Rev. Lett. **94**, 173001 (2005)
15. J.O. Hirschfelder, C.F. Curtiss, R.B. Bird, *Molecular Theory of Gases and Liquids* (J. Wiley, New-York, 1954), pp. 955-964
16. W. Li, I. Mourachko, M.W. Noel, T.F. Gallagher, Phys. Rev. A **67**, 052502-1 (2003)
17. M.L. Zimmerman, M.G. Littman, M.M. Kash, D. Kleppner, Phys. Rev. A **20**, 2251 (1979)
18. C. Monroe, W. Swann, H. Robinson, C. Wieman, Phys. Rev. Lett. **65**, 1571 (1990)
19. F. Robicheaux, J.D. Hanson, Phys. Rev. Lett. **88**, 055002 (2002)
20. F. Robicheaux, J.D. Hanson, Phys. Plasmas **10**, 2217 (2003)